Template for APEX (Jan. 2014)

A 271.8 nm deep-ultraviolet laser diode for room temperature operation

Ziyi Zhang[1,3*], Maki Kushimoto[2], Tadayoshi Sakai[2], Naoharu Sugiyama[3], Leo J. Schowalter[3,4], Chiaki Sasaoka[3], and Hiroshi Amano[3]

[1]*Innovative Devices R&D Center, Corporate Research & Development, Asahi Kasei Corporation, Fuji, Shizuoka 416-8501, Japan*

[2]*Graduate School of Engineering, Nagoya University, Furo-cho, Chikusa-ku, Aichi 464-8603, Japan*

[3]*Center for Integrated Research of Future Electronics, Institute of Materials Research and System for Sustainability, Nagoya University, Furo-cho, Chikusa-ku, Aichi 464-8601, Japan*

[4]*Crystal IS, 70 Cohoes Avenue, Green Island, NY 12183, U.S.A.*

E-mail: zhang.zc@om.asahi-kasei.co.jp

We present a deep-ultraviolet semiconductor laser diode that operates under current injection at room temperature and at a very short wavelength. The laser structure was grown on the (0001) face of a single-crystal aluminum nitride substrate. The measured lasing wavelength was 271.8 nm with a pulsed duration of 50 ns and a repetition frequency of 2 kHz. A polarization-induced doping cladding layer was employed to achieve hole conductivity and injection without intentional impurity doping. Even with this undoped layer, we were still able to achieve a low operation voltage of 13.8 V at a lasing threshold current of 0.4 A.

Ultraviolet (UV) laser diodes (LDs) operating at wavelengths of the UV-C region (100 ~ 280 nm) are potential enabling devices for a number of applications, such as bio-/chemical sensing, small particle detection, disinfection, medical treatment and surface monitoring. Since the breakthrough on epitaxial growth of group-III nitrides demonstrated the potential for low-cost semiconductor UV light emitting devices,[1)] enormous efforts have been made on developing UV light emitting diodes (LEDs).[2)] These UV LEDs have already demonstrated wavelengths down to 210 nm, deep into the UV-C.[3)] On the other hand, UV LDs have only been demonstrated in the wavelength span of UV-A (315 ~ 400 nm).[4-10)] New technical issues have been encountered in attempts to shorter lasing wavelengths. For instance, while UV LEDs have successfully been demonstrated on foreign substrates such as SiC or sapphire, the relatively thick layers with high Al concentration required for LDs cause high dislocation densities and even crack formation which can significantly degrade the internal quantum efficiency (IQE) of the active layer.[11)] This issue can be well addressed by using single crystal aluminum nitride (AlN) as the epitaxial substrate.

Indeed, AlN has already been considered as a promising epitaxial growth substrate for the UV-C laser. It was demonstrated that nearly 1.0 μm of a pseudomorphic AlGaN layer, with an Al content of 0.7, could be grown on a single-crystal AlN substrate,[12)] to preserve the low dislocation density of the substrate. Active layers, grown on single-crystal AlN substrates, were proven preferable in achieving high IQE[13-14)] values, as well as large optical gain in the UV-C region.[15)] A remarkably low threshold pumping power density for stimulated emission via optical pumping has also been demonstrated on high quality AlN substrates.[16-20)] However, the development of a UV-C LD also requires the development of a thick, low absorption AlGaN layers (with high Al-content) needed for optical confinement. At the same time, these optical confinement layers, or cladding layers, need to be highly conductive to achieve the relatively high current densities needed for laser operation. This is particularly difficult for hole transport since the hole conductivity decreases with increasing Al content in the AlGaN alloy.[21-23)] In the past years, various techniques have been reported to obtain increased p-type conductivity for high Al-containing AlGaN, such as the distributed polarization doping (DPD)[24-27)] and short period superlattice (SPSL)[28-30)] methods.

There are several conceivable advantages of the DPD employment as the p-cladding layer in the UV-C LD. By using a continuous grade in the alloy composition of the AlGaN in the DPD approach, a higher hole conductivity can be expected when compared to the SPSL method. In addition, for growth of the Al-polar surface, the DPD approach will

generate holes when graded from high Al concentration to low Al concentration. Thus, this approach can also be designed to serve simultaneously as the electron blocking layer,[25] avoiding the need for an additional electron blocking layer that could potentially hinder the hole injection. Moreover, the DPD layer is expected to be highly optically transparent in spite of being a highly conductive hole layer since it achieves this high conductivity without impurity doping.[27] As one might expect, it has been found doping of the p-side of the cladding layer with Mg may cause significant modal loss and increase the threshold pumping power density required for stimulated emission.[31]

In this letter, we demonstrate the development of a UV-C LD fabricated on a single crystal AlN substrate, which operates under pulsed current at room temperature, employing a DPD structure.

The LD structure was epitaxially grown using the metal organic chemical vapor deposition method, on a (0001)-orientated, high-quality, 2-inch single-crystal AlN substrate, with a dislocation density of $10^3 \sim 10^4$ cm^{-2}. The AlN substrate was provided by Crystal IS. The grown laser structure consisted of: (i) a 0.4 μm AlN regrowth; (ii) a 0.35 μm n-type $Al_{0.7}Ga_{0.3}N$:Si as the n-side cladding; (iii) a 9.0 nm single quantum well layer emitting at 270 nm, which was sandwiched between 50 nm n-side and p-side $Al_{0.63}Ga_{0.37}N$ waveguide layers to define the optical mode with a theoretically calculated confinement factor of 2.9 %; (iv) a 0.32 μm thick $Al_xGa_{1-x}N$ DPD layer with an Al composition that decreased from x = 1.0 to 0.7 in the growth direction of the p-side; and (v) a contact layer including a p-type AlGaN:Mg with Al composition grading down to GaN and a p-type GaN:Mg. No intentional impurity doping was applied during the waveguides and DPD layer growth. The n-side cladding and contact layer were doped with impurity concentration over 1×10^{19} cm^{-3}. All the AlGaN layers were confirmed to be pseudomorphically grown on the single-crystal AlN substrate, using the reciprocal space mapping of (11-24) plane X-ray diffraction technique. The LD structure was then partially etched to expose the n-type layer and shaped a 4 μm-width ridge stripe along the <1-100> direction that would allow the current confinement. SiO_2 was deposited as a passivation layer, followed by vanadium-based n-electrode, nickel/gold-based p-electrode and pad metal formation on the exposed n-side cladding and contact layer. The whole electrode formation process was carried out using the facilities of the Center for Integrated Research of Future Electronics, Transformative Electronics Facilities (C-TEFs) of the Nagoya University. A schematic cross section of the fabricated device structure is illustrated in Figure 1.

The fabricated stripe with the electrode was then cleaved along the <11-20>

direction to form a 400 μm-long laser cavity with atomically flat (1-100) facets at either end. This was followed by the deposition of 5 pairs HfO_2/SiO_2 multilayers[18] on both of the cleaved facets which achieved a high reflectivity (>90%) and that ultimately reduced the threshold current.

The electrical characteristics of the LD were measured under a 50 ns pulsed current injection in a time period of 0.5 ms (duty 0.01%) at room temperature. The edge emission was measured simultaneously with a photon multimeter and a spectrometer, and the obtained spectrum was split, via a Glan-Thompson prism polarizer, to transverse electric (TE) ($E\perp<0001>$) and transverse magnetic (TM) ($E//<0001>$) modes.

Figure 2 shows the current-voltage (I-V) and the emission power features, evaluated by the photon multimeter, as a function of the pulsed forward current (I-L) of the fabricated device. Non-linear increase of the output power was observed at a forward current above 0.4 A, which corresponded to 25 kA/cm^2, considering that the current flow was restricted to the area of the p-electrode. A sharp lasing spectrum peak clearly emerged at around 271 nm above the threshold current. The inset in Figure 2 depicts the edge emission spectrum measured by the spectrometer under a 0.5 A forward current. The operating voltage at the threshold current was 13.8 V. Figure 3 shows the measured edge emission spectra of the TE and TM polarization components at currents (a) above and (b) below threshold. The inset of Figure 3(a) shows the TE component with the highest wavelength resolution. The spontaneous emission of the TE and TM components, observed at a current of 0.2 A, showed a full-width-at-half-maximum (FWHM) value of 6.6 nm and 11 nm, respectively. The TE component was sharp and dominant with a FWHM value of 0.41 nm at 0.5 A forward current, while the FWHM value of the TM component did not change (11 nm). The remarkably low operating voltage of 13.8 V at threshold current should be attributed to the step-less (continuous gradient) valence band profile of the DPD. The region with the highest Al content, adjacent to the p-side waveguide, probably served as an electron blocking layer and enhanced the hole injection. The pseudomorphic growth of the whole structure, including the DPD on the single-crystal AlN substrate, maximized the polarization-induced charge to achieve high hole conductivity, considering that relaxation of the graded structure can also hinder polarization doping.[32]

Another obstacle that deteriorated LD characteristics was the convex, hexagonal pyramid shaped hillock (HPH) feature that appeared after the epitaxial growth, with a density of 6×10^3 cm^{-2}, as shown in the inset optical microscope image of Figure 4(a). An additional

longer wavelength emission peak at 278 nm clearly emerged for devices where HPHs were observed in the p-electron region, like device-A (Figure 4(a)). Lasing was only achieved with devices without p-electrode overlapping an HPH, like device-B (Figure 4(b)). Similar features of luminescence have been reported by other groups for AlGaN layers.[33] Cross section transmission electron microscopy (TEM) observations appear to demonstrate that HPHs can originate from existing threading dislocation in the single-crystal AlN substrate. Threading dislocations can provide a non-radiative recombination center[11] in the active layer, as well as non-uniform current injection. Guiding mode scattering may also occur at devices which overlap an HPH, leading to additional internal loss and to lasing inhibition. Consequently, a high-quality AlN substrate with low dislocation density appears to be fundamental to the development of a UV-C LD.

In conclusion, we have demonstrated a UV-C LD fabricated on a single-crystal AlN substrate operating at room temperature. Lasing was achieved at a wavelength of 271.8 nm under pulse current injection above the threshold current (0.4 A), which corresponded to a current density of 25 kA/cm^2. An undoped DPD was employed as the p-side to achieve low internal loss, high hole conductivity, and high hole injection. Furthermore, the graded valence band profile of the DPD contributed to a remarkably low operating voltage of 13.8 V at the threshold current. To our knowledge, the current-injection LD reported here operates at the shortest wavelength reported so far.

Acknowledgments

The authors would like to acknowledge Prof. Yoshio Honda of Nagoya University, Mr. Kazuhiro Nagase, and Dr. Naohiro Kuze of Asahi Kasei Corporation for their invaluable discussion and considerable support. The authors would also like to acknowledge Dr. Nishii and working members of C-TEFs for their great contribution to development of laser diode process.

References

1) H. Amano, N. Sawaki, I. Akasaki, and Y. Toyoda, Appl. Phys. Lett. **48**, 353 (1986)

2) M. Kneissl, T.Y. Seong, J. Han and H. Amano, Nat. Photonics **13**, 233 (2019)

3) Y. Taniyasu, M. Kasu, and T. Makimoto, Nature **441**, 325 (2006)

4) I. Akasaki, S.Sota, H. Sakai, T. Tanaka, M. Koike and H. Amano, Electron. Lett. **32**, 1105 (1996)

5) K. Iida, T. Kawashima, A. Miyazaki, H. Kasugai, S. Mishima, A. Honshio, Y. Miyake, M. Iwaya, S. Kamiyama, H. Amano and I. Akasaki, Jpn. J. Appl. Phys. **43**, L499 (2004)

6) S. Masui, Y. Matsuyama, T. Yanamoto, T. Kozaki, S. Nagahama and T. Mukai, Jpn. J. Appl. Phys. **42**, L1318 (2003)

7) M. Kneissl, D. W. Treat, M. Teepe, N. Miyashita, and N. M. Johnson, Appl. Phys. Lett. **82**, 4441 (2003)

8) M. Kneissl, Z. Yang, M. Teepe, C. Knollenberg, O. Schmidt, P. Kiesel, N. M. Johnson, S. Schujman and L. J. Schowalter, J. Appl. Phys. **101**, 123103 (2007)

9) H, Yoshida, Y. Yamashita, M. Kuwabara, and H. Kan, Nat. Photonics **2**, 551 (2008)

10) Y. Aoki, M. Kuwabara, Y. Yamashita, Y. Takagi, A. Sugiyama, and H. Yoshida, Appl. Phys. Lett. **107**, 151103 (2015)

11) K. Ban, J. Yamamoto, K. Takeda, K. Ide, M. Iwaya, T. Takeuchi, S. Kamiyama, I. Akasaki, and H. Amano, Appl. Phys. Express **4**, 052101 (2011)

12) S. G. Mueller, R. T. Bondokov, K. E. Morgan, G. A. Slack, S. B. Schujman, J. Grandusky, J. A. Smart, and L. J. Schowalter, Phys. Status Solidi A **206**, 1153 (2009)

13) Z. Bryan, I. Bryan, J. Xie, S. Mita, Z. Sitar, and R. Collazo, Appl. Phys. Lett. **106**, 142107 (2015)

14) J. R. Grandusky, J. Chen, S. R. Gibb, M. C. Mendrick, C. G. Moe, L. Rodak, G. A. Garrett, M. Wraback, and L. J. Schowalter, Appl. Phys. Express **6**, 032101 (2013)

15) W. Guo, Z. Bryan, J. Xie, R. Kirste, S. Mita, I. Bryan, L. Hussey, M. Bobea, B. Haidet, M. Gerhold, R. Collazo, and Z. Sitar, J. Appl. Phys. **115**, 103108 (2014)

16) T. Wunderer, C. L. Chua, Z. Yang, J. E. Northrup, N. M. Johnson, G. A. Garrett, H. Shen, and M. Wraback, Appl. Phys. Express **4**, 092101 (2011)

17) Z. Lochner, T. T. Kao, Y. S. Liu, X. H. Li, M. M. Satter, S. C. Shen, P. D. Yoder, J. H. Ryou, R. D. Dupuis, Y. Wei, H. Xie, A. Fischer, and F. A. Ponce, Appl. Phys. Lett. **102**, 101110 (2013)

18) T. T. Kao, Y. S. Liu, M. M. Satter, X. H. Li, Z. Lochner, P. D. Yoder, T. Detchprohm,

R. D. Dupuis, S. C. Shen, J. H. Ryou, A. M. Fischer, Y. Wei, H. Xie and F. A. Ponce, Appl. Phys. Lett. **103**, 211103 (2013)

19) M. Martens, F. Mehnke, C. Kuhn, C. Reich, V. Kueller, A. Knauer, C. Netzel, C. Hartmann, J. Wollweber, J. Rass, T. Wernicke, M. Bickermann, M. Weyers, and M. Kneissl, IEEE Photon. Technol. Lett. **26**, 342 (2014)
20) R. Kirste, Q. Guo, J. H. Dycus, A. Franke, S. Mita, B. Sarkar, P. Reddy, J. M. LeBeau, R. Collazo, and Z. Sitar, Appl. Phys. Express **11**, 082101 (2018)
21) M. Katsuragawa, S. Sota, M. Komori, C. Anbe, T. Takeuchi, H. Sakai, H. Amano, and I. Akasaki, J. Cryst. Growth **189**, 528 (1998)
22) M. L. Nakarmi, N. Nepal, J. Y. Lin, and H. X. Jiang, Appl. Phys. Lett. **94**, 091903 (2009)
23) T. Kinoshita, T. Obata, H. Yanagi, and S. Inoue, Appl. Phys. Lett. **102**, 012105 (2013).
24) D. Jena, S. Heikman, D. Green, D. Buttari, R. Coffie, H. Xing, S. Keller, S. DenBarrs, J. S. Speck, U. K. Mishra, and I. Smorchkova, Appl. Phys. Lett. **81**, 4395 (2002)
25) J. Simon, V. Protasenko, C. Lian, H. Xing, D. Jena, Science **327**, 60 (2009)
26) R. Dalmau, and B. Moody, ECS Trans. **86**, 31 (2018)
27) S. Li, M. Ware, J. Wu, P. Minor, Z. Wang Z. Wu, Y. Jiang, and G. J. Salamo, Appl. Phys. Lett. **101**, 122103 (2012)
28) B. Cheng, S. Choi, J. E. Northrup, Z. Yang, C. Knollenberg, M. Teepe, T. Wunderer, C. L. Chua, and N. M. Johnson, Appl. Phys. Lett. **102**, 231106 (2013)
29) K. Ebata, J. Nishinaka, Y. Taniyasu, and K. Kumakura, Jpn. J. Appl. Phys. **57**, 04FH09 (2018)
30) M. Martens, C. Kuhn, E. Ziffer, T. Simoneit, V. Kueller, A. Knauer, J. Rass, T. Wernicke, S. Einfeldt, M. Weyers, and M. Kneissl, Appl. Phys. Lett. **108**, 151108 (2016)
31) M. Martens, C. Kuhn, T. Simoneit, S. Hagedorn, A. Knauer, T. Wernicke, M. Weyers, and M. Kneissl, Appl. Phys. Lett. **110**, 081103 (2017)
32) T. Yasuda, T. Takeuchi, M. Iwaya, S Kamiyama, I. Akasaki, and H. Amano, Appl. Phys. Express **10**, 025502 (2017)
33) W. C. Ke, C. S. Ku, H. Y. Huang, W. C. Chen, L. Lee, W. K. Chen, W. C. Chou, W. H. Chen, M. C. Lee, W. J. Lin, Y. C. Cheng, and Y. T. Cherng, Appl. Phys. Lett. **85**, 3047 (2004)

Figure Captions

Fig. 1. Schematic drawing of the fabricated UV-C LD structure.

Fig. 2. I-V and edge emission I-L characteristics of measured UV-C LD. The inset figure shows the edge emission spectrum at 0.5 A forward current.

Fig. 3. Edge emission spectra with TE and TM polarization at (a) 0.5 A and (b) 0.2 A forward current. The inset figure in (a) shows the spectrum of the TE mode at 0.5 A with the highest wavelength resolution.

Fig. 4. Comparison of the (a) edge emission spectra at 0.3 A forward current and (b) I-V, I-L characteristic of two adjacent devices; A: with, and B: without p-electrode stepping on HPHs. The inset picture in (a) shows the optical microscope image of both devices. Circles indicate HPHs that overlapped with the p-electrode. Arrows indicate probe scratches.

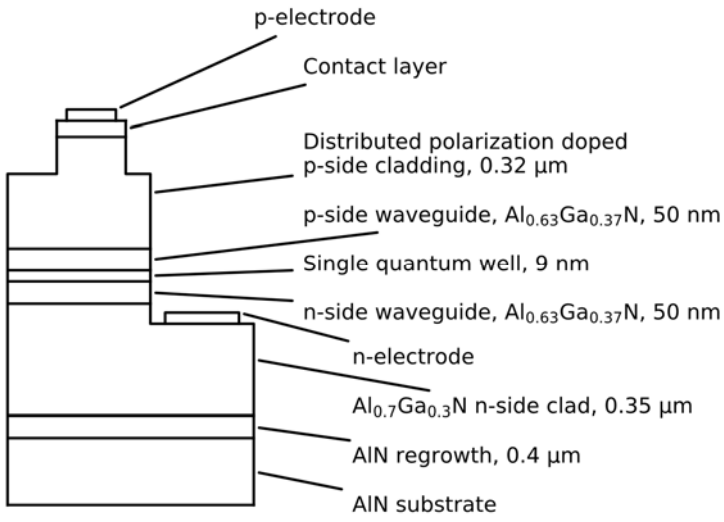
p-electrode
Contact layer
Distributed polarization doped
p-side cladding, 0.32 µm
p-side waveguide, $Al_{0.63}Ga_{0.37}N$, 50 nm
Single quantum well, 9 nm
n-side waveguide, $Al_{0.63}Ga_{0.37}N$, 50 nm
n-electrode
$Al_{0.7}Ga_{0.3}N$ n-side clad, 0.35 µm
AlN regrowth, 0.4 µm
AlN substrate

Fig. 1.

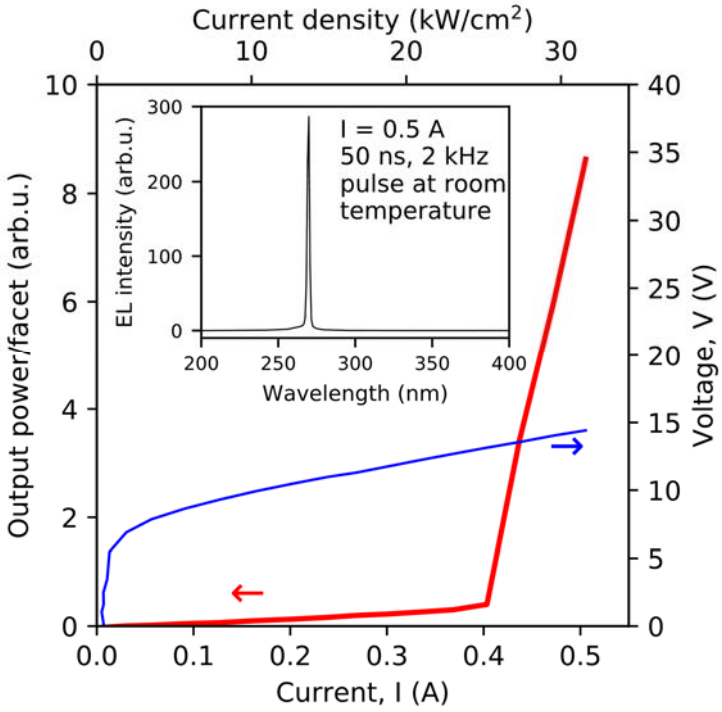
Current density (kW/cm²)
0
10
20
30
Output power/facet (arb.u.)
Voltage, V (V)
Current, I (A)
0.0
0.1
0.2
0.3
0.4
0.5
EL intensity (arb.u.)
Wavelength (nm)
200
250
300
350
400
I = 0.5 A
50 ns, 2 kHz
pulse at room
temperature

Fig. 2.

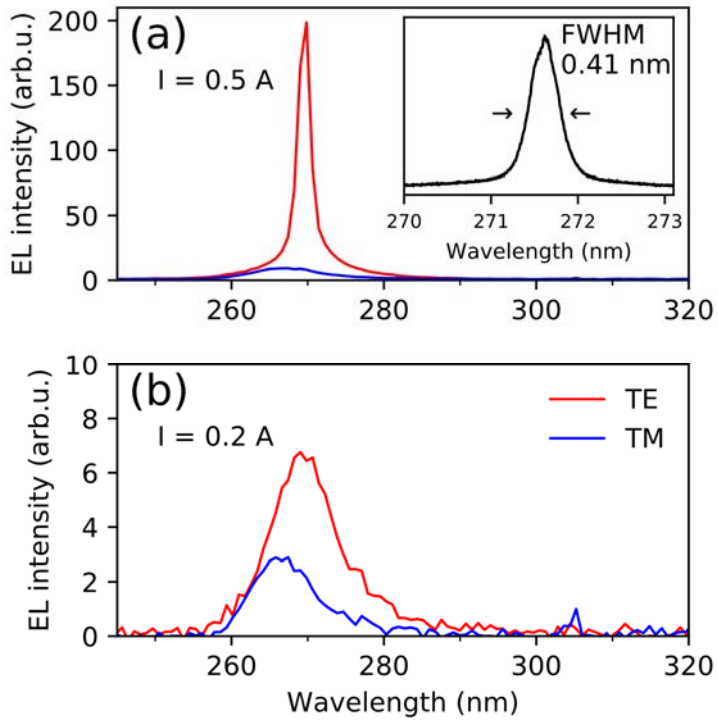
(a)
I = 0.5 A
FWHM
0.41 nm
EL intensity (arb.u.)
Wavelength (nm)
(b)
I = 0.2 A
TE
TM
EL intensity (arb.u.)
Wavelength (nm)

Fig. 3.

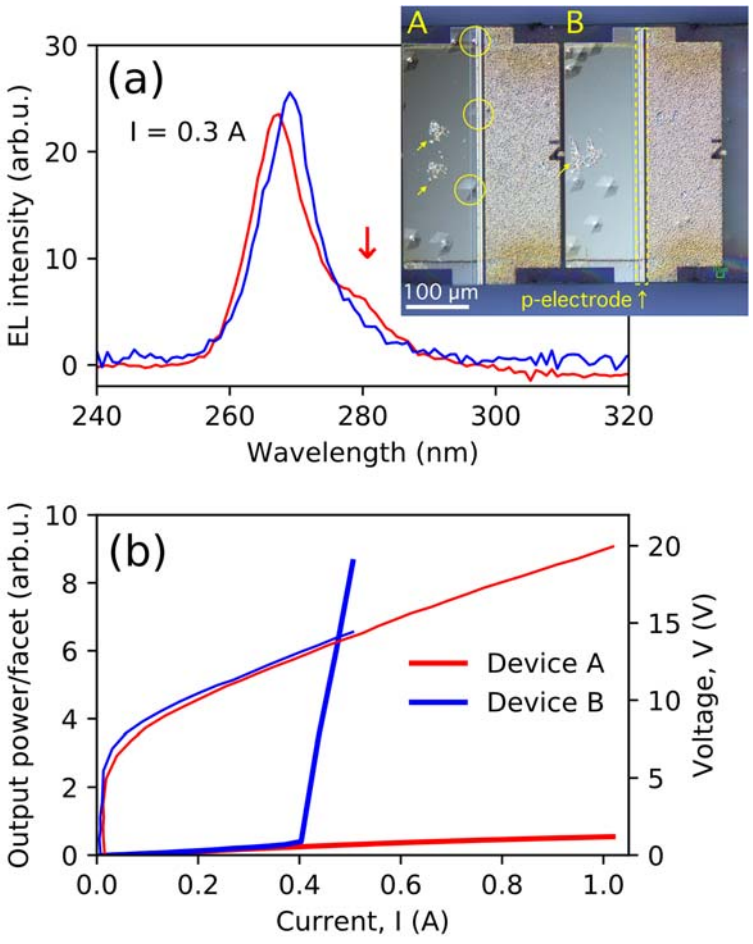
(a)
I = 0.3 A
A
B
100 μm
p-electrode
EL intensity (arb.u.)
Wavelength (nm)
(b)
Device A
Device B
Output power/facet (arb.u.)
Voltage, V (V)
Current, I (A)

Fig. 4.